H_2S PHOTODEGRADATION BY TiO_2/M-MCM-41 (M=Cr or Ce): DEACTIVATION AND BY-PRODUCT GENERATION UNDER UV-A AND VISIBLE LIGHT

Raquel Portela[a], Maria C. Canela[b], Benigno Sánchez[a], Fabielle C. Marques[b], Alexandre M. Stumbo[b], Ronan F. Tessinari[b], Juan M. Coronado[a], Silvia Suárez[a]

a) CIEMAT-PSA-Environmental Applications of Solar Radiation. Madrid, Spain.

b) UENF-CCT-Laboratório de Ciências Químicas. Campos dos Goytacazes-RJ, Brazil.

E-mail: raquel.portela@ciemat.es, mccanela@gmail.com

ABSTRACT

M-MCM-41 molecular sieves (M = Ce or Cr) were prepared by a hydrothermal method and impregnated with TiO_2. The materials were characterized by XRD, N_2 adsorption-desorption, DRS and XPS. Their potential application to photooxidize H_2S in a wet gas stream was tested in a continuous flow reactor operating at a flow rate of 110 $mL \cdot min^{-1}$ at 50% relative humidity and using 30 ppm_v of the pollutant. The photocatalytic efficiency using UV-A and visible-light was compared to the activity of TiO_2/MCM-41 without heteroatoms incorporated into the MCM-41 structure. It was found that the incorporation of Ce did not improve the performance of TiO_2/MCM-41, but Cr-containing samples presented higher initial efficiency and were able to photooxidize H_2S without formation of SO_2 as a by-product, in contrast to the other prepared samples and to Degussa P-25 TiO_2. Moreover, no other gaseous by-product was detected. The isomorphic incorporation of Cr into the structure of MCM-41 followed by TiO_2 incorporation produced photocatalysts that presented good adsorption capacity and were much more active under visible-light than under UV-light. This performance represents an important advantage for solar applications. Their photoactivity depended on the concentration of chromium; the highest efficiency was attained with samples with a Si/Cr ratio of 50. Finally, deactivation was observed as a consequence of sulfate accumulation on the surface of the catalyst and reduction of Cr^{6+}.

KEY WORDS: H_2S, MCM-41, Cr, Ce, mesoporous, photocatalysis, visible light, deactivation.

1 INTRODUCTION

Most research about heterogeneous photocatalysis uses TiO_2-anatase nanoparticles, which are known to absorb radiation below 387 nm (band gap energy = 3.2 eV). TiO_2 may take advantage of just the UV-A range of the solar spectrum, which represents only 3-6% of the total solar radiation. In addition, the low photonic efficiency of TiO_2 [1] further limits its overall usefulness. As a result, artificial illumination is usually required and, consequently, the full potential of photocatalysis as a cheap and clean technology is not completely realized. Therefore, a great deal of attention has been devoted to design visible light-activated materials to improve the photocatalytic systems [2] by approaches such as TiO_2 doping with metal ions [3], N [4], C [5] or S [6]; semiconductor coupling [7] or even the search for alternative TiO_2-free photocatalysts [8]. In this direction, mesoporous M41S molecular sieves modified by incorporation of transition metals have been tested recently in heterogeneous photocatalysis.

MCM-41 is the most attractive member of the M41S family because of its hexagonal array of uniform pores with adjustable diameter (15 to 100 Å) and high surface area (typically > 1000 $m^2.g^{-1}$) [9]. The isomorphic incorporation of transition metals into the MCM-41structure and impregnation with TiO_2 produces catalysts active under visible light [10]. In addition to acting as a support to control the dispersion and local structure of the active sites, molecular sieves have other useful properties such as the condensation effect for reactant gases or the shape selectivity due to the pore structure and restricted molecular-scale size [11]. Finally, the MCM-41 structure can enhance the interaction between TiO_2 and the transition metal, which is directly correlated to photoactivity. The good synergy between TiO_2 and Cr-MCM-41 has been recently demonstrated in the destruction of organic pollutants in aqueous phase [12]. The authors have proved the possibility of using this material also in gas phase photocatalysis in the elimination of

thiophene [13]. The use of TiO_2/Cr-MCM-41 in gas phase eliminates the problem of Cr leaching and improves the environmental significance of these materials [14].

The potential role of gas phase photocatalysis in the removal of malodorous and toxic compounds has been demonstrated by several authors [15-20]. One of the most targeted sulfur compounds to degrade is H_2S, a widespread chemical released as by-product of many processes, such as sour gas flaring, petroleum refining, pulp and paper manufacturing or wastewater treatment. H_2S has a very low odor threshold, 0.5 ppb_v [21], and the Threshold Limit Values -Short Term Exposure Limit (TLV-STEL) and Time-Weighted Average (TLV-TWA)- are 10 and 15 ppm_v, respectively, in most European countries [22]. Although widely used, commercial H_2S removal techniques such as biofiltration and bioscrubbing [23], wet chemical scrubbing [24], incineration [25] and adsorption [26] are not optimal solutions. In fact, these techniques lack long-term stability, are non-destructive or require high chemicals and energy consumption. In contrast, the known advantages of photocatalysis make this technology very attractive. However, an important barrier to the full application of photocatalysis is the chemical nature of the pollutant and, consequently, of the reaction products. On one hand, most pollutants containing S (hydrogen sulfide, sulfur dioxide, dimethyl sulfide, dimethyl disulfide, carbon disulfide, carbonyl sulfide) or other heteroatoms such as N, P [27] or Si [28, 29], are capable of promoting irreversible deactivation of the photocatalyst. For compounds containing sulfur, accumulation of sulfate as the final oxidation product may deactivate the photocatalyst [30, 31]. On the other hand, a strategy to avoid deactivation could be limiting the photodegradation to reactions releasing gaseous oxidation products instead of depositing sulfate, but all gaseous sulfur compounds are toxic, corrosive and malodorous and therefore not recommended as final products of a treatment [32]. In our previous research with sol-gel TiO_2 and UV light, the feasibility of H_2S photocatalytic removal was confirmed [33]. Nevertheless, sulfate was found to accumulate on the surface deactivating the catalyst. Moreover, although Canela and collaborators did not find any reaction product besides sulfate [34] and Kataoka and

collaborators found only a small amount of SO_2 attributed to sources other than photoreaction [35], Portela and collaborators have found, with both TiO_2 and TiO_2-ZrO_2 photocatalysts, that SO_2 was a reaction product [20]. The formation of sulfur dioxide has been observed during the photooxidation of other sulfur compounds. For instance, Nishikawa and Takahara observed its formation during tests with dimethyl sulfide [36].

In this study, we test the potential application of M-MCM-41 (M = Ce or Cr) molecular sieves impregnated with TiO_2 to destruct H_2S via photocatalysis using UV and visible light. The effect of the molecular sieve and the incorporated heteroatoms in the selectivity of the reaction and the nature of the catalyst deactivation is studied.

2 MATERIALS AND EXPERIMENTAL

2.1 Synthesis of photocatalysts based on MCM-41

M-MCM-41 (M = Ce or Cr) molecular sieves were prepared using a hydrothermal method adapted from [37]. $CrCl_3 \cdot 6H_2O$ (Vetec, 97%) and $CeCl_3 \cdot 7H_2O$ (Vetec, 99%) were used as metallic precursors and tetraethylortosilicate (TEOS; Fluka, 99%) as source of silicon. In order to prepare samples with atomic ratio Si/M = ∞ (no heteroatom), 100, 50 and 25, the metallic precursors were added to a N-cetyl-N,N,N-trimethylammonium chloride solution (CTACl; Aldrich, 25% w/w) under stirring. After 30 minutes, tetramethylammonium hydroxide solution (TMAOH; Fluka, 25% w/w) was added dropwise under stirring. After addition of tetraethylortosilicate (TEOS; Fluka, 99%), the resulting mixture was stirred for 1.5 h. The molar ratio SiO_2:CTACl:TMAOH:H_2O:M (Cr_2O_3 or CeO_2) was 1:0.40:0.26:25:*x* (where *x* = 0, 0.01, 0.02 or 0.04). The final mixture, with pH values between 11 and 12, was treated under autogenous pressure without stirring at 135^{o}C for 14 hours in a steel autoclave internally lined with Teflon. The resulting solids were filtered, washed with distilled water until pH 7 was reached, and dried in an oven at 90^{o}C for 12 hours. The template was removed by calcination

under N_2 flow at 540°C for 1 hour (heating rate of $2^oC \cdot min^{-1}$) followed by 5 hours under airflow at the same temperature.

The resulting materials were impregnated with 20 wt% of TiO_2 obtained by hydrolysis of titanium (IV) isopropoxide (Aldrich, 97%). The molecular sieve (typically 1.0 g) was suspended in 80 mL of isopropyl alcohol (Synth, p.a.) and the proper amount of $Ti(OPr^i)_4$ was added to achieve 20 wt% of TiO_2. The suspension was stirred at ambient temperature and 1 mL of water was added dropwise. After 1 h the solvent was evaporated by heating at 50°C. The samples were dried in an oven for 1 h at 90°C and calcined at 450°C under airflow for 4 h.

In Table 1 are listed the different prepared samples (the number in brackets is the Si/M ratio) together with the sample P25-SiO_2, prepared for comparative purposes by mixing commercial SiO_2 (Merck) and TiO_2 (Degussa P-25). When the samples have been used in photocatalytic tests with either visible or ultraviolet-A radiation the suffix “VIS” or “UVA” was added..

2.2 Characterization of synthesized photocatalysts

This study used N_2 physisorption to determine surface area and pore size distribution with a Quantachrome Autosorb 1C. All samples were degassed for 1 h at 300°C under vacuum before analysis. Surface areas and pore size distributions were determined using BET (*P/P_0 = 0.05-0.30*) and BJH methods, respectively, both through Autosorb for Windows® software, version 1.24. Diffuse reflectance spectra (DRS) in the range of 200-800 nm were recorded by a Varian spectrophotometer equipped with ISR1200 integrating sphere attachment using $BaSO_4$ as reference. X-Ray Diffraction analysis were performed by means of an X´Pert Pro PANalytical automatic diffractometer, using Cu Kα radiation (λ = 0.154 nm) with a Ni filter. Low angle measurements were performed in the 2θ range from 0.4º to 8º with a step size of 0.02º and a step time of 20 s.

X-ray photoelectron spectra (XPS) were obtained with a VG Escalab 200R spectrometer fitted with a monochromated Mg Kα radiation ($h\nu$ = 1253.6 eV) 120 W X-ray source and a hemispherical electron analyzer. The powdered samples were placed on a sample rod and

introduced in a pre-treatment chamber to be degassed at 25ºC and 10^{-3} Pa for 5 hours prior to their transfer to the analysis chamber. Residual pressure during data acquisition was maintained below $3 \cdot 10^{-7}$ Pa. The energy regions of the photoelectrons of interest (Cr 2p, Ti 2p, Si 2s, O 1s, S 1s), were scanned several times to provide an acceptable signal-to-noise ratio. Accurate binding energies (± 0.2 eV) were determined by referring to the C1s peak at 284.9 eV.

2.3 Photocatalytic activity tests

The photocatalytic tests were performed in a steel tubular reactor (d_{int} = 18.2 mm) illuminated by an internal 8W lamp placed in axial position (d_{ext} = 15.2 mm). OSRAM L8W/954 was used for tests made with visible light (emission maximum at around 460 nm, 540 nm and 615 nm) and PHILIPS TL8W/05 FAM for tests made with UV light (emission maximum at 365 nm). 200 mg of photocatalyst were placed in the thin annular volume between the lamp and the reactor wall (thickness: 3 mm). The catalyst occupied a length of 10 mm and was held in place by plugs of glass wool. A continuous inlet gas stream with a flow rate of 110 $mL \cdot min^{-1}$, 30 ppm_v of H_2S and 50% relative humidity at 30ºC entered the reactor. This procedure implied a residence time of 0.43 s and a space time (calculated as catalyst load to molar flow rate ratio) of $8 \cdot 10^{10}$ $mg \cdot s \cdot mol^{-1}$. H_2S was supplied from a certified H_2S/N_2 cylinder (Air Liquide) and diluted with wet air. The desired concentrations of pollutant, H_2O and O_2 (20 % ±1) in the air were attained by means of liquid and gas mass flow controllers, in a system that has already been reported [33]. The analysis of the gaseous compounds was performed using a Micro-GC Varian CP-4900 equipped with a micro thermal conductivity detector (μ-TCD) and a CP-PoraPlotQ column (10 m x 0.15 mm). The concentration of the continuous inlet gas stream was measured in by-pass until stabilization before each run. The gas stream was then passed through the reaction system in dark conditions. The lamp was turned on only when the adsorption equilibrium was reached (the H_2S concentration was higher than 95% of the by-pass value).

3 RESULTS AND DISCUSSION

3.1 Characterization of synthesized photocatalysts

3.1.1. XRD studies and N_2 adsorption isotherms

Low angle XRD patterns of these materials showed a peak at 2θ values of about 2º in all cases, as shown in Figure 1 for some representative samples. This peak can be indexed to the (100) reflection of the hexagonal array of pores characteristic of MCM-41 phase [38]. However, the relatively low intensity of this feature, coupled with the absence of the weaker high-index peaks, indicates that the MCM structure was not completely ordered, and therefore the existence of some amorphous domains in our samples was highly likely. In contrast with other studies [39, 40] the incorporation of Cr or Ce is not clearly detrimental for the crystallinity of our samples because, as displayed in Figure 1, the intensity of the (100) peak presents similar or higher intensity for samples containing metals than for the pure siliceous molecular sieve. The unit cell parameter of the hexagonal cell, a_0, can be calculated from the spacing of the (100) planes, d_{100}, according to the equation $a_0 = 2d_{100}/\sqrt{3}$ [40]. The results obtained for these samples were summarized in Table 1. The data indicate that the incorporation of Cr slightly increased the unit cell, while Ce addition had the opposite effect. Although the increment of the M-O distance with respect to Si-O is expected to yield an increment of a_0, the opposite tendency has been observed as well [39], as specific synthesis conditions may affect wall thickness.

Figure 1

Meanwhile, TiO_2 incorporation was studied by high angle (20-80º 2θ) XRD measurements. The obtained results revealed the formation of TiO_2-anatase, whose pattern is overlapped with the broad amorphous halo of SiO_2 at about 23.4º. However, there is no obvious indication of the presence of other metal oxides. The crystallite size of TiO_2 for samples with and without Cr or Ce estimated by the Scherrer equation was summarized in Table 1. These results show that Cr incorporation results in anatase crystals of smaller diameter, which could be caused by an easier nucleation on the metal-modified surface of the molecular sieve.

The N_2 physisorption isotherms are of type IV, according to IUPAC classification, a typical pattern of mesoporous structures [41]. All samples exhibited complementary textural- and framework-confined mesoporosity, which was evidenced by the presence of two separate and well-defined hysteresis loops. Isotherm profiles were not modified by TiO_2 impregnation. The formation of larger pores in samples containing chromium or cerium was associated to the formation of defects (or distortions) in the molecular sieve structure (Table 1). The surface area decreased with the amount of chromium and cerium in the samples. The same trend has been reported in the literature [42].

Table 1

3.1.2. Diffuse reflectance spectroscopy – UV-Vis

Figure 2 shows UV-Vis spectra of Cr-MCM-41 and Ce-MCM-41 impregnated with 20 wt% TiO_2. Chromium-containing materials showed absorption beginning at approximately 600 nm, while samples without chromium absorbed light only in the UV-range. The presence of the heteroatom apparently reduced the band-gap energy from the 3.2 eV value found for pure TiO_2 to ≈2.0 eV. These results demonstrate that the synthesized materials have a great potential as photocatalysts capable of using solar light. DRS spectrum of calcined Cr-MCM-41(100) has two intense bands at 275 and 390 nm, attributed to $O(2p) \rightarrow Cr^{6+}(3d^0)$ charge transfer of chromate (CrO_4^{2-}) species, that indicate chromium oxidation to Cr(VI) during calcination [43], [39]. Moreover, d-d transition of Cr^{5+} occurs in the same spectral region. The band at 440 nm may be assigned to octahedral Cr^{3+} ions which indicate the presence of Cr^{3+} in the calcined sample, even under calcination temperatures of 630ºC. Rodrigues et al. detected Cr^{3+} species on Cr-MCM-41 [38]. The band at 440 nm may also be attributed to the forbidden charge transfer band of dichromate species [44]. In our study such process was difficult to observe due to the overlap with TiO_2 adsorption band, after the impregnation. A band at ≈350 nm confirmed the formation of anatase TiO_2 in chromium and cerium-containing materials. Band coincidence between TiO_2 and chromate species indicates that the absorption in the range of 370-500 nm could be related to a heterojunction of titania and chromium. The spectra of chromium-containing samples

showed an absorption band around 700 nm in the red region of the electromagnetic spectrum assigned to d-d transitions described as $^4A_{2g}(F) \rightarrow {}^4T_{2g}(F)$ from Cr^{3+} in octahedral coordination [45]. The cerium-containing materials showed an absorption band below 300 nm attributed to the electronic transition from oxygen to cerium for a tetra-coordinated Ce^{4+} ($O^{2-} \rightarrow Ce^{4+}$) [42]. The absorption in the visible region was very weak and no absorption was detected above 500 nm.

Figure 2

3.1.3. X-ray photoelectron (XPS) analysis

Samples with different Cr content were analyzed by X-Ray photoelectron spectroscopy. The energy regions for Cr2p, Ti2p, Si2p, O1s and S1s were analyzed for all the samples. The Ti 2p3/2 region showed a band centered at 458.5eV with a satellite peak at 464.2 eV characteristic of TiO_2-anatase. The binding energy for Si2p core level was found at 103.3 eV, corresponding to SiO_2. In Figure 3a and 3b the Cr2p and O1s spectra for samples with atomic ratio Si/Cr=100 and Si/Cr=25 are displayed and the surface atomic ratios calculated for Cr-containing samples are collected in Table 2. The analysis of the Cr2p3/2 region showed the presence of two different Cr species or chemical states on the catalysts surface with maxima centered at 576.6 eV and 579.0 eV, corresponding to Cr^{3+} and Cr^{6+} species, respectively. The presence of these two species has been observed previously with other supports [46]. The deconvolution of the O1s spectra showed two bands, centered at 532.7 eV and 529.7 eV. The former corresponded to oxygen from SiO_2 [47] and the latter assigned to the combination of oxygen species from TiO_2 and CrO_x [48]. As expected, higher SiO_2 content in TiO_2/Cr-MCM-41(100) resulted in higher contribution of the O1s band centered at 532.7 eV. The sample with Si/Cr=25 presented the highest Cr/Ti ratio and also a greater amount of Cr^{+3}, in agreement with Sun et al., who found that samples with smaller Si/Cr ratio contained mixed oxidation states and therefore lower Cr^{+6}/Cr_{total} [14] Nevertheless, considering the Cr/Ti ratio calculated by XPS and the Si/Cr theoretical ratio, the results suggest the formation of extraframework Cr, probably as Cr_2O_3, reducing the metal dispersion on TiO_2/Cr-MCM-41(25).

Figure 3

In order to verify whether there was any influence of the irradiation and radiation type on the oxidation state of superficial species, XPS analysis of some samples were performed after reactions using visible and UV-A lamps (Figure 4). A band centered at 168.7 eV was detected now in the S1s spectra. According to the literature, this band was assigned to sulfate species [49]. A dependence of the S/Ti ratio with the Cr content in the sample was found (Table 2). On the other hand, the photocatalytic reaction promoted an increase of the Cr^{3+}/Cr_{total} ratio in all the studied cases, due to the reduction of Cr^{6+} to Cr^{3+}. Moreover, UV-A radiation, more energetic than visible radiation, practically caused the total reduction to Cr^{3+}. The decrease of the Cr/Ti ratio after the catalytic test was probably due to the deposition of sulfate over the Cr species.

Figure 4

3.2 Adsorption capacity of the samples

The adsorption capacity of the different catalysts under dynamic conditions in wet air was measured before the photocatalytic tests. The H_2S adsorption capacity was very low when no heteroatom was incorporated into the structure of the molecular sieves. However, the adsorption capacity improved with the amount of chromium (Figure 4), despite a decrease in the surface area. Previous studies reported the use of hydrogen sulfide to reduce Cr(VI) to Cr(III) species [50]. Therefore, considering that these samples contain a significant amount of Cr^{6+}, as revealed by XPS analysis, H_2S could initially reduce part of the chromate present in Cr-containing molecular sieves. Nevertheless, this process does not lead to the total reduction of the chromate species present in the samples, as the study of the used catalysts indicates. This fact could be related with the presence of different monochromate/polychromate species in the molecular sieve after calcination [44, 51].

Figure 5

It has been performed one test in the absence of humidity in order to verify a possible competition for the adsorption sites between water and hydrogen sulfide. Our results confirmed

this fact since H_2S adsorption capacity in the dark dropped drastically when humidity was present in the continuous gas stream (Figure 6, left). Once the catalyst surface was saturated, it was irradiated in order to eliminate H_2S photocatalitically. The humidity did not seem to affect the photocatalytic activity (Figure 6, right).

Figure 6

3.3 Photocatalytic activity

A blank test (without catalyst) demonstrated the absence of homogeneous photolysis of H_2S. In Figure 7 a typical photocatalytic test is shown. When a constant concentration by-passing the reactor is reached, the polluted wet gas stream is passed through the reactor in the dark, until the adsorption drops below 5% of the H_2S in the feed. Then the light is turned on. Around 30 minutes, in the case of the UV-A–lamp, or 45 minutes, in the case of the visible-lamp, are necessary to reach the new adsorption equilibrium, due to the progressive temperature increase produced during the lamp initialization, which causes water and H_2S desorption.

Figure 7

3.3.1 Photocatalytic activity with UV-A light

Figure 8 shows the evolution of the photoactivity during 6 hours of UV irradiation of TiO_2/M-MCM-41 molecular sieves (M = Ce or Cr, Si/M = 50 and 100) compared to the TiO_2-MCM-41 molecular sieve (without heteroatom) and to a mixture of commercial SiO_2 and TiO_2 with the same TiO_2 content (20% w/w). The latter presented the highest conversion, 80%, and no deactivation occurred within 3 hours. Despite the higher surface area of the molecular sieves, P25-SiO_2 was more efficient in the degradation of H_2S than TiO_2 impregnated on MCM-41. The higher efficiency in H_2S degradation of P-25 from Degussa can be explained by the synergic effect of anatase and rutile allotropic forms present in this material, an effect widely described in the literature [52, 53], while TiO_2 added to MCM-41 is present only in the anatase form.

Figure 8

Among the molecular sieves, the one without heteroatom converted 33% of the H_2S and no deactivation occurred during 24 hours; the addition of Ce did not seem to improve this performance. The incorporation of Cr at the adequate concentration (Si/Cr = 50) had two different effects: the initial conversion rate was enhanced and the deactivation was faster. This results can be adequately explained by observing the formation of SO_2 during the photoreaction (Figure 9), which is the only gaseous product detected during H_2S photocatalytic degradation [20].

Figure 9

With P25-SiO_2 most of the H_2S was converted into SO_2, which was desorbed and released with the outlet gas stream. Therefore, deactivation did not occur, but the degradation product into which the pollutant was converted is both toxic and corrosive. On the other hand, during tests with TiO_2/Cr-MCM-41 samples, no gaseous products containing sulfur were detected. Sulfate or elemental sulfur, the most likely reaction products, would accumulate on the surface of the photocatalyst covering the active sites and, therefore, lead to a progressive loss of activity. In the case of TiO_2/MCM-41 and TiO_2/Ce-MCM-41, SO_2 appeared in the outlet gas stream after some minutes of reaction, corroborating previous results on the same subject [20].

In addition to the deactivation caused by products accumulation, the influence of Cr^{6+} reduction on this process, according to XPS results, must not be ignored. Sun et al. have reported that TiO_2/Cr-MCM-41 catalysts deactivate gradually during 4-chlorophenol degradation under visible light due to Cr^{6+} reduction [14]. These authors have also found that reduced chromium in the photocatalyst can be completely reoxidized by heating the catalyst at 450ºC for 3 hours. Davydov et al. have found the same kind of deactivation and confirmed the progressive reduction of Cr^{6+} to Cr^{3+} and Cr^{2+} [10].

3.3.2. Photocatalytic activity with visible light

Samples containing Cr show light absorption above 400 nm (see Figure 2), indicating that they might show photocatalytic activity under visible light. Figure 10 shows the photoactivity of the molecular sieves with Si/Cr ratios of ∞ (no Cr), 100, 50 and 25. As expected, the sample without chromium was unable to photodegrade H_2S under visible light, while samples containing chromium were very active photocatalytically, 2-3 times more active than under UVA-light. Nevertheless, it has been found that the sample with Si/Cr=50 was more active than the samples with Si/Cr=25 or 100. This result indicates that there is an optimal amount of chromium for these photocatalysts. According to XPS results, the sample with higher metal loading presented higher S/Ti ratio, indicating that probably the extra-framework Cr_2O_3 favored the formation of sulfate and, in addition to the lower surface area and higher content of Cr^{3+}, the faster catalyst deactivation. Cr-MCM-41(50) sample showed very low conversion of H_2S, which was attributed to the fast reduction of Cr^{6+} [50]. Davydov et al. have shown that the interaction of Cr^{6+} and TiO_2 is essential for the activity of the photocatalyst, because it allows the charge transfer transition $Cr^{6+}=O^{2-} \rightarrow (Cr^{5+}-O^{-})^{*}$, which is promoted by visible light [10]. Therefore, Cr^{5+} species can probably donate an electron to the neighboring TiO_2. Meanwhile, the O^{-} of the photoexcited chromate species can withdraw electrons from the TiO_2 particles, leaving an oxidant hole in the valence band during the decay process.

Ce-containing samples impregnated with TiO_2 did not show any activity in the visible light, as expected due to the scarce absorption in the visible range (see Figure 2).

Figure 10

3.3. Discussion

H_2S was converted either into sulfate, which accumulated on the surface deactivating the catalyst, or as previous studies [33] into both sulfate and SO_2, toxic and corrosive compound which was desorbed and released with the outlet gas stream, depending on the incorporation of Cr or not to the molecular sieves. In the first case, the reaction may take place using visible light

at even higher reaction rate than using UV-A-light, which enables the reaction activation by solar energy.

TiO_2/M-MCM-41 samples are equally active in the presence or absence of water vapor, which may be related to the higher surface area and to the large amount of Si-OH available in the molecular sieves than the supported TiO_2 used in previous studies, where higher initial photoactivity and faster deactivation of the catalyst were observed with dry inlet gas streams [20] compared to streams containing water vapor [33].

The presence of Cr^{6+} on the catalysts was essential to carry out the photocatalytic reaction, but low Cr concentration (Si/Cr ≥ 50) favors the conversion. Cr^{6+} was reduced to Cr^{3+} during the photocatalytic process, according to XPS results before and after the photocatalytic test, probably by the electrons accumulated on the catalyst surface. Therefore the increase of Cr^{3+} concentration was one reason for the catalysts deactivation. According to Rodrigues et al., during the degradation of trichloroethylene, Cr^{6+}/Cr^{5+} were the only photospecies susceptible to absorb visible-wavelength photons, whereas with UV light Cr^{3+} species were also active [38]. Davydov et al. [10] observed that Cr^{6+} was essential for the reaction using visible light, since its fully reduced form did not exhibit any photoactivity, but the role of Cr^{3+} was not clear, even if the deactivated catalysts were rich in Cr^{3+}.

The catalysts deactivation was mainly caused by the reduction of Cr^{6+} to Cr^{3+} and the blockage of active sites due to the accumulation of sulfate on the catalysts surface. Nevertheless this deactivation may be reversible. Sun et al. pointed out that the reduced chromium in 25% TiO_2/Cr-MCM-41 can be reoxidized to Cr^{6+} by calcination at 450ºC and under this circumstance the catalyst regeneration would be achieved [14]. We have analyzed a 20% TiO_2/Cr-MCM-41 deactivated sample by thermogravimetry-mass spectrometry (TG-MS) and the formation of sulfur species (SO and SO_2) with a maximum at 460ºC indicates that sulfate may be decomposed by calcination as well.

4 CONCLUSIONS

MCM-41 molecular sieves with incorporated Cr or Ce and impregnated with TiO_2 (20% w/w) showed high efficiency to photooxidize H_2S in gas phase.

Among the prepared photocatalysts tested, the highest H_2S conversion was obtained by the use of TiO_2/Cr-MCM-41 and visible light. TiO_2/Cr-MCM-41 degraded H_2S with either UV- or visible-light and did not generate any other toxic gaseous product, such as SO_2, which is a problem when the samples without Cr incorporation or TiO_2 P-25 from Degussa are used. Nevertheless, the catalyst deactivated with time due to the reduction of Cr^{6+} to Cr^{3+} and the blockage of active sites by sulfate accumulation on the surface. The photoactivity depended on chromium concentration and the optimal Si/Cr ratio was found to be 50.

The incorporation of Ce to the structure of the molecular sieves has neither improved their performance, nor avoided SO_2 formation or extended the activity to the visible range.

5 ACKNOWLEDGMENTS

The authors would like to acknowledge Comunidad de Madrid (DETOX-H2S S-0505/AMB/0406) and Fundación Carolina for the funding and IQ-Unicamp for DRS-UV-Vis analysis. We would also like to thank Dr. Rojas for his help in the interpretation of the XPS results.

6 REFERENCES

[1] M.R. Hoffmann, S.T. Martin, W. Choi, D.W. Bahnemann, Chem. Rev. 95 (1995) 69-96.
[2] M. Anpo, M. Takeuchi, J. Catal. 216 (2003) 505-516.
[3] W. Choi, A. Termin, M.R. Hoffmann, J. Phys. Chem. 98 (1994) 13669-13679.
[4] R. Asahi, T. Morikawa, T. Ohwaki, K. Aoki, Y. Taga, Science 293 (2001) 269-271.
[5] H. Irie, Y. Watanabe, K. Hashimoto, Chem. Lett. 32 (2003) 772-773.
[6] T. Umebayashi, T. Yamaki, H. Itoh, K. Asai, Appl. Phys. Lett. 81 (2002) 454-456.
[7] N. Keller, E. Barraud, F. Bosc, D. Edwards, V. Keller, Appl. Catal. B 70 (2007) 423-430.
[8] M. Hara, G. Hitoki, T. Takata, J.N. Kondo, H. Kobayashi, K. Domen, Catal. Today 78 (2003) 555-560.
[9] C.T. Kresge, M.E. Leonowicz, W.J. Roth, J.C. Vartuli, J.S. Beck, Nature 359 (1992) 710-712.
[10] L. Davydov, E.P. Reddy, P. France, P.G. Smirniotis, J. Catal. 203 (2001) 157-167.
[11] M. Matsuoka, M. Anpo, J. Photochem. Photobiol. C 3 (2003) 225-252.
[12] B. Sun, E.P. Reddy, P.G. Smirniotis, J. Catal. 237 (2006) 314-321.
[13] F.C. Marques, M.C. Canela, A.M. Stumbo, Catal. Today 133-135 (2008) 594-599.
[14] B. Sun, E.P. Reddy, P.G. Smirniotis, Appl. Catal. B 57 (2005) 139-149.

[15] M.C. Canela, R.M. Alberici, R.C.R. Sofía, M.N. Eberlin, W.F. Jardim, Environ.Sci.Technol. 33 (1999) 2788-2792.
[16] A.V. Vorontsov, E.V. Savinov, L. Davydov, P.G. Smirniotis, Appl. Catal. B 32 (2001) 11-24.
[17] C. Cantau, S. Larribau, T. Pigot, M. Simon, M.T. Maurette, S. Lacombe, Catal. Today 122 (2007) 27-38.
[18] C. Guillard, D. Baldassare, C. Duchamp, M.N. Ghazzal, S. Daniele, Catal. Today 122 (2007) 160-167.
[19] K. Demeestere, J. Dewulf, B. De Witte, H. Van Langenhove, Appl. Catal. B 60 (2005) 93-106.
[20] R. Portela, B. Sánchez, J.M. Coronado, JAOTs 10 (2007) 375-380.
[21] B. Mills, Filtration & Separation 32 (1995) 146-152.
[22] INSHT, (2007) 234.
[23] S.J. Park, S.I. Nam, E.S. Choi, Water Sci. Technol. 44 (2001) 301-308.
[24] P. Hardy, J.E. Burgess, S. Morton, R.M. Stuetz, Water Sci. Technol. 44 (2001) 189-196.
[25] M.Y. Shin, D.W. Park, J.S. Chung, Catal. Today 63 (2000) 405-411.
[26] F. Adib, A. Bagreev, T.J. Bandosz, Environ. Sci. Technol. 34 (2000) 686-692.
[27] M. Kerzhentsev, C. Guillard, J.-M. Herrmann, P. Pichat, Catal. Today 27 (1996) 215-220.
[28] J. Peral, D.F. Ollis, J. Mol. Catal. A: Chem. 115 (1997) 347-354.
[29] R.-D. Sun, A. Nakajima, T. Watanabe, K. Hashimoto, J. Photochem. Photobiol. A 154 (2003) 203-209.
[30] N. González-García, J.A. Ayllon, X. Domenech, J. Peral, Appl. Catal. B 52 (2004) 69-77.
[31] C.P. Chang, J.N. Chen, M.C. Lu, H.Y. Yang, Chemosphere 58 (2005) 1071-1078.
[32] P.N.L. Lens, J.G. Kuenen, Water Sci. Technol. 44 (2001) 57-66.
[33] R. Portela, B. Sanchez, J.M. Coronado, R. Candal, S. Suarez, Catal. Today 129 (2007) 223-230.
[34] M.C. Canela, R.M. Alberici, W.F. Jardim, J. Photochem. Photobiol. A 112 (1998) 73-80.
[35] S. Kataoka, E. Lee, M.I. Tejedor-Tejedor, M.A. Anderson, Appl. Catal. B 61 (2005) 159-163.
[36] H. Nishikawa, Y. Takahara, J. Mol. Catal. A: Chem. 172 (2001) 247-251.
[37] T. Blasco, A. Corma, M.T. Navarro, J.P. Pariente, J. Catal. 156 (1995) 65-74.
[38] S. Rodrigues, K.T. Ranjit, S. Uma, I.N. Martyanov, K.J. Klabunde, J. Catal. 230 (2005) 158-165.
[39] Z. Zhu, Z. Chang, L. Kevan, J. Phys. Chem. B 103 (1999) 2680-2688.
[40] S.H. Park, B.H. Kim, M. Selvaraj, T.G. Lee, J. Ind. Eng. Chem. 13 (2007) 637-643.
[41] M. Yates, in: M. Faraldos, C. Goberna (Eds.), Técnicas de análisis y caracterización de materiales, Biblioteca de Ciencias, CSIC, Madrid, 2002, pp. 221-246.
[42] S.C. Laha, P. Mukherjee, S.R. Sainkar, R. Kumar, J. Catal. 207 (2002) 213-223.
[43] B.M. Weckhuysen, R. Ramachandra Rao, J. Pelgrims, R.A. Schoonheydt, P. Bodart, G. Debras, O. Collart, P. Van Der Voort, E.F. Vansant, Chem.-Eur. J. 6 (2000) 2960-2970.
[44] B.M. Weckhuysen, I.E. Wachs, R.A. Schoonheydt, Chem. Rev. 96 (1996) 3327-3349.
[45] M.P. McDaniel, J. Catal. 76 (1982) 37-47.
[46] C.M. Pradier, F. Rodrigues, P. Marcus, M.V. Landau, M.L. Kaliya, A. Gutman, M. Herskowitz, Appl. Catal. B 27 (2000) 73-85.
[47] B.M. Reddy, I. Ganesh, E.P. Reddy, J. Phys. Chem. B 101 (1997) 1769-1774.
[48] B.M. Reddy, B. Chowdhury, E.P. Reddy, A. Fernández, J. Mol. Catal. A: Chem. 162 (2000) 423-433.
[49] C.D. Wagner, W.M. Riggs, L.E. Davis, J.F. Moulder, Handbook of X-ray Photoelectron Spectra, 1st ed., Perkin–Elmer Corporation, Eden Prairie, MN, 1979.
[50] J.A. Rodriguez, S. Chaturvedi, M. Kuhn, J. Van Ek, U. Diebold, P.S. Robbert, H. Geisler, C.A. Ventrice Jr., J. Chem. Phys. 107 (1997) 9146-9156.
[51] F.C. Marques, M.C. Canela, A.M. Stumbo, Catal. Today In Press (2008).
[52] R.I. Bickley, T. González-Carreño, J.S. Less, L. Palmisano, R.J.D. Tilley, J. Solid State Chem. 92 (1991) 178-190.

[53] C. Wu, Y. Yue, X. Deng, W. Hua, Z. Gao, Catal. Today 93-95 (2004) 863-869.

Figure captions

Figure 1. XRD patterns at low (A) and high (B) angle of the samples a) MCM-41, b) TiO_2/Cr-MCM-41(100) and c) TiO_2/Cr-MCM-41(50). The star marks a peak of the sample holder, while "a" stands for the anatase peaks.

Figure 2. DRS-UV-Vis spectra of the molecular sieves modified with Ce (left) and Cr (right).

Figure 3. XPS spectra of the core levels for TiO_2/Cr-MCM-41 samples with different Cr loading a) Cr2p b) O1s

Figure 4. XPS spectra of the core levels for fresh and used samples: a) Cr 2p and b) O1s

Figure 5. Adsorption of H_2S in the dark as a function of chromium content. Si/Cr = ∞ (●), 100 (●), 50 (●) and 25 (○).

Figure 6. Behavior of TiO_2/Cr-MCM-41(50) sample in the dark (left) and during irradiation with UVA light after saturation (right) with wet (•) or dry (•) inlet gas streams.

Figure 7. H_2S (▬) and water (▬) during visible-light test with TiO_2/Cr-MCM-41(50) sample.

Figure 8. H_2S conversion over time under UV-A light for P25-SiO_2 (—), TiO_2/MCM-41 (—), TiO_2/Ce-MCM-41(100) (▪▪▪), TiO_2/Ce-MCM-41(50) (▪▪▪), TiO_2/Cr-MCM-41(100) (▲) and TiO_2/Cr-MCM-41(50) (▲)

Figure 9. SO_2 generation during H_2S UV-photooxidation with TiO_2/MCM-41 (●), TiO_2/Ce-MCM-41(100) (●), and TiO_2P25-SiO_2 (○). During tests with TiO_2/Cr-MCM-41(100) no SO_2 was detected under neither UV light nor visible light.

Figure 10. H_2S conversion under visible light for MCM-41 with 20% TiO_2 (black) and without TiO_2 (gray) after 45 minutes (-○-) and 180 minutes (·△·) of illumination.

Table 1. Results of textural and structural characterization of the photocatalysts.

Sample	Si/M	TiO_2 (%)	BET (m^2/g)	Pore size (Å)	Pore volume (cm^3/g)	Unit cell parameter a_0 (Å)	TiO_2 size (nm)
P25-SiO_2	∞	20	51	-	-	-	23.0
TiO_2/MCM-41	∞	20	1068	22	0.54	49	13.3
TiO_2/Ce-MCM-41(100)	100	20	724	24	0.64	43	14.2
TiO_2/Ce-MCM-41(50)	50	20	542	23	0.57	48	8.9
TiO_2/Cr-MCM-41(100)	100	20	823	24	0.62	51	7.0
TiO_2/Cr-MCM-41(50)	50	20	557	29	0.60	52	6.9
TiO_2/Cr-MCM-41-(25)	25	20	316	18		-	-

Table 2. Surface atomic ratios calculated for Cr-containing samples.

	Cr/Ti	**Cr^{3+}/Cr total (%)**	**S/Ti**
TiO_2/Cr-MCM-41(100)	0.34	60	-
TiO_2/Cr-MCM-41(100)VIS	0.16	75	0.05
TiO_2/Cr-MCM-41(100)UVA	0.12	94	0.06
TiO2/Cr-MCM-41(25)	0.45	67	-
TiO2/Cr-MCM-41(25)VIS	0.42	77	0.13

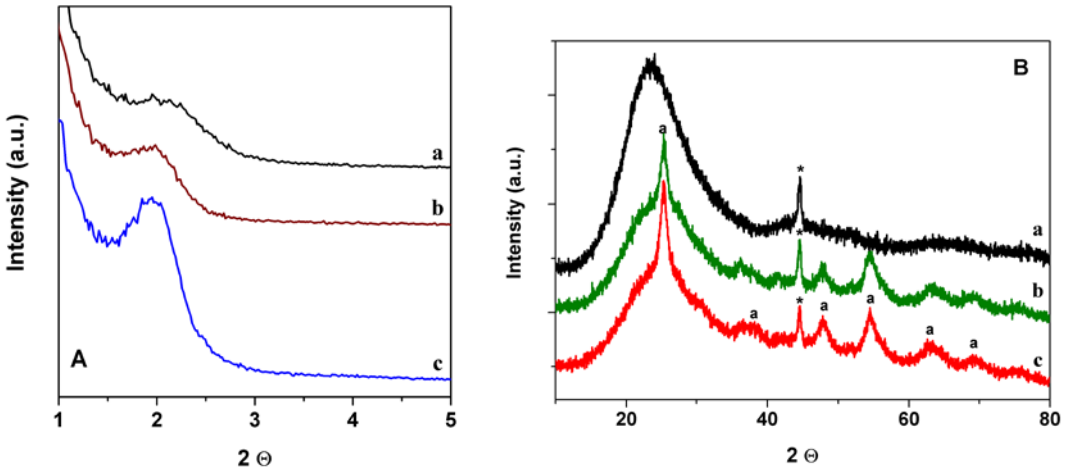
Intensity (a.u.)
A
a
b
c
1
2
3
4
5
2 Θ
B
Intensity (a.u.)
a
b
c
*
20
40
60
80
2 Θ

Figure 2

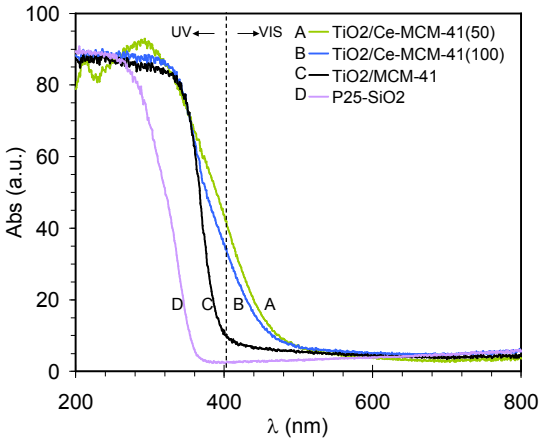
UV
VIS
A TiO2/Ce-MCM-41(50)
B TiO2/Ce-MCM-41(100)
C TiO2/MCM-41
D P25-SiO2
Abs (a.u.)
λ (nm)
0
20
40
60
80
100
200
400
600
800
D
C
B
A

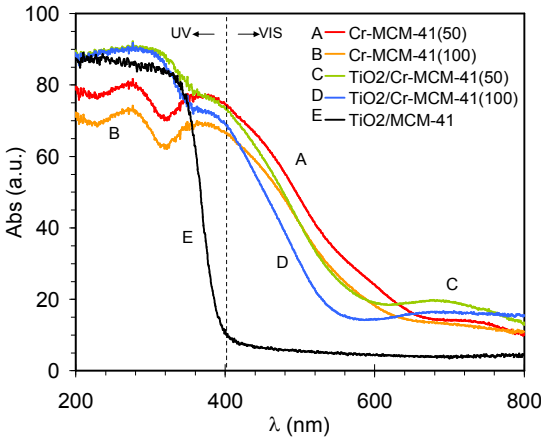
UV
VIS
A Cr-MCM-41(50)
B Cr-MCM-41(100)
C TiO2/Cr-MCM-41(50)
D TiO2/Cr-MCM-41(100)
E TiO2/MCM-41
Abs (a.u.)
λ (nm)
0
20
40
60
80
100
200
400
600
800
A
B
C
D
E

Figure 3

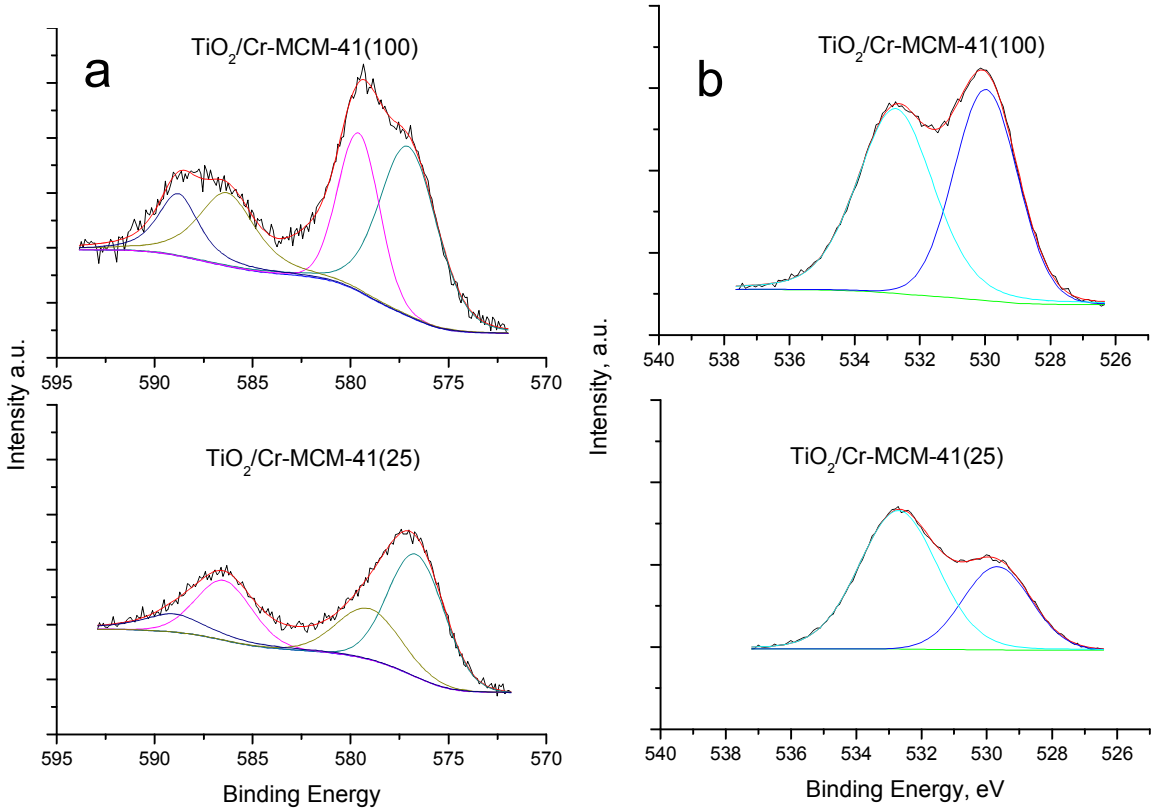
a
TiO2/Cr-MCM-41(100)
TiO2/Cr-MCM-41(25)
Intensity a.u.
595
590
585
580
575
570
Binding Energy
b
TiO2/Cr-MCM-41(100)
TiO2/Cr-MCM-41(25)
Intensity, a.u.
540
538
536
534
532
530
528
526
Binding Energy, eV

Figure 4

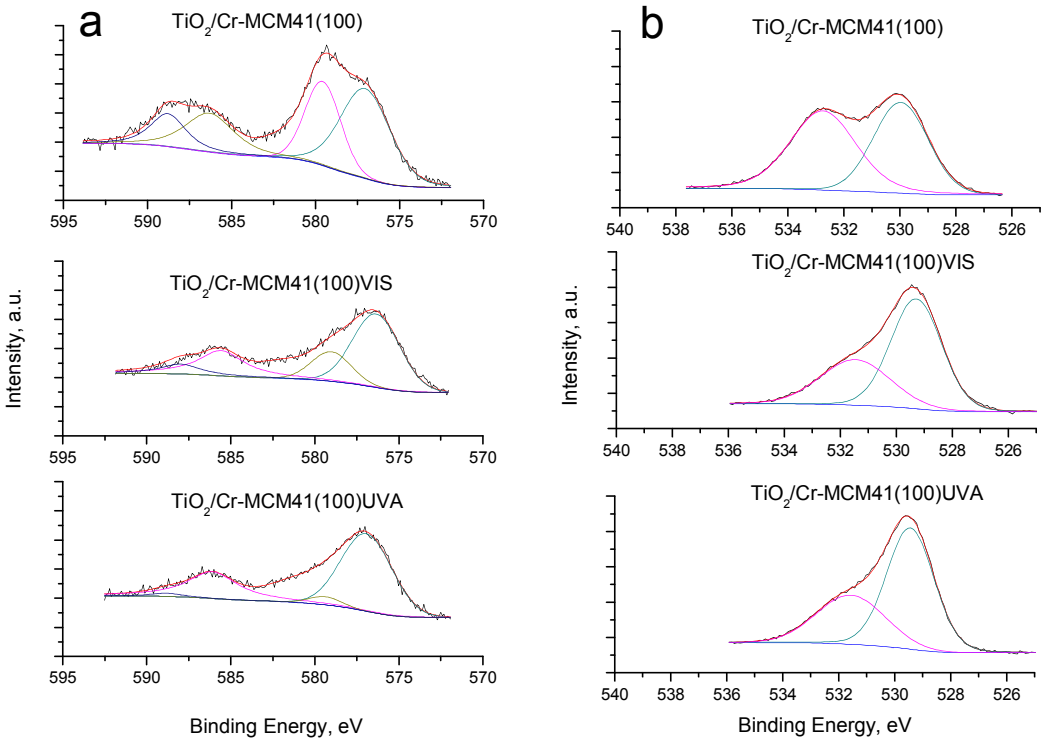
a
TiO2/Cr-MCM41(100)
TiO2/Cr-MCM41(100)VIS
TiO2/Cr-MCM41(100)UVA
595 590 585 580 575 570
Intensity, a.u.
Binding Energy, eV
b
TiO2/Cr-MCM41(100)
TiO2/Cr-MCM41(100)VIS
TiO2/Cr-MCM41(100)UVA
540 538 536 534 532 530 528 526
Intensity, a.u.
Binding Energy, eV

Figure 5

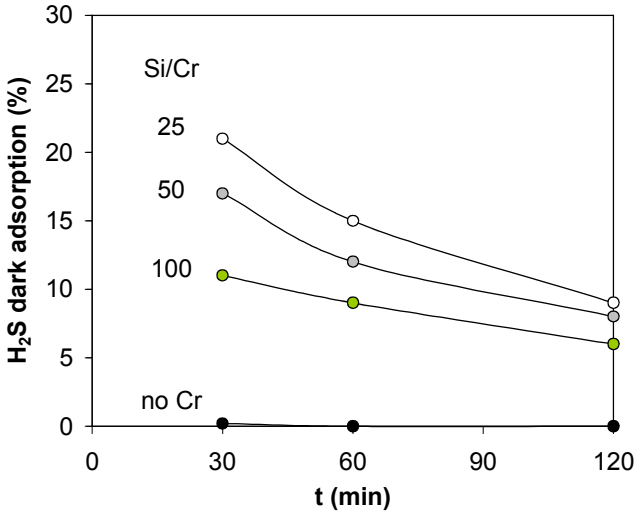
30
25
20
15
10
5
0
Si/Cr
25
50
100
no Cr
H2S dark adsorption (%)
0
30
60
90
120
t (min)

Figure 6

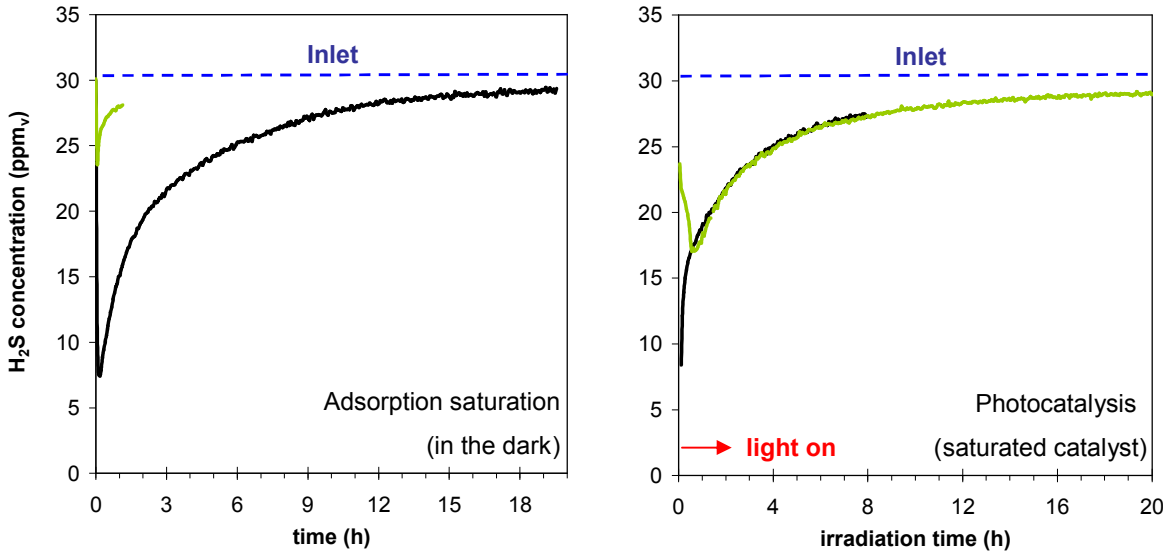
Inlet
Adsorption saturation
(in the dark)
H_2S concentration (ppm_v)
time (h)
Inlet
Photocatalysis
(saturated catalyst)
light on
irradiation time (h)

Figure 7

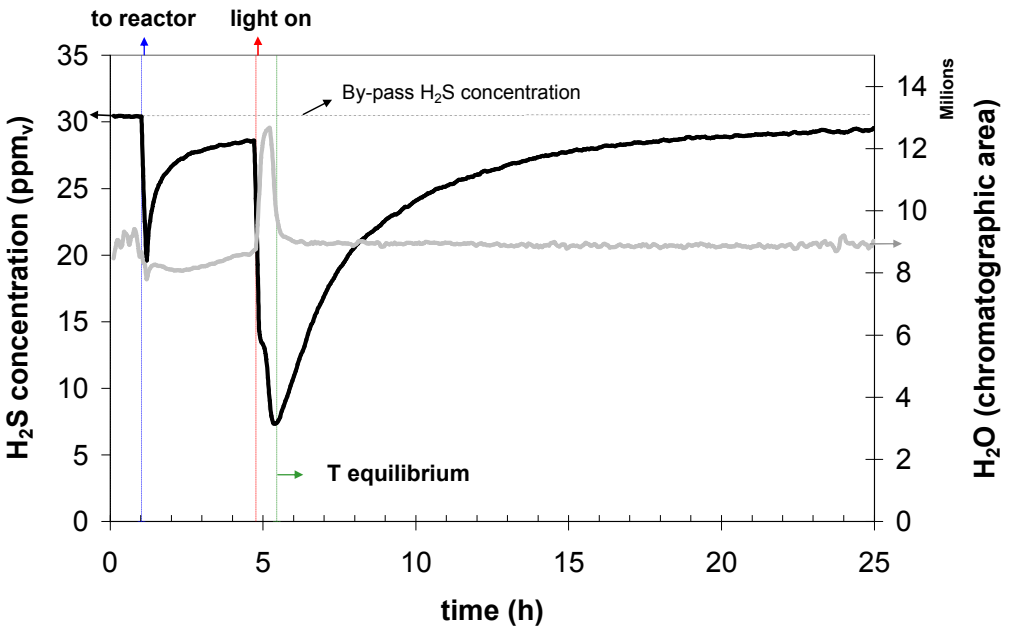
to reactor
light on
By-pass H_2S concentration
T equilibrium
H_2S concentration (ppm_v)
H_2O (chromatographic area)
Millions
time (h)
0
5
10
15
20
25
30
35
0
2
4
6
8
10
12
14

Figure 8

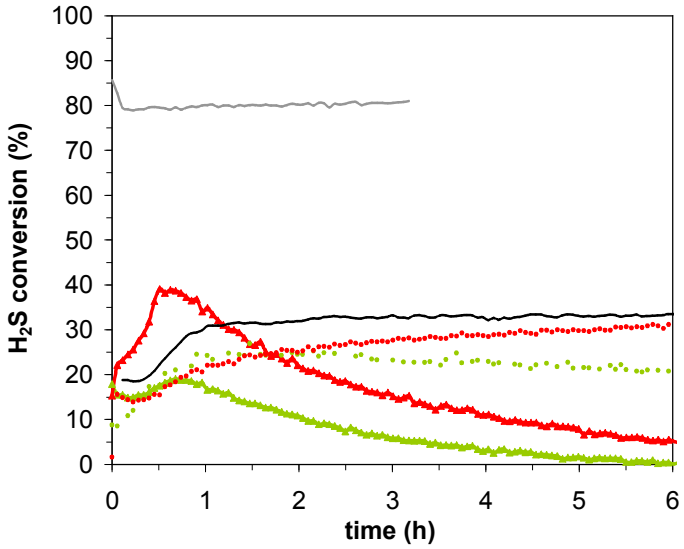

Figure 9

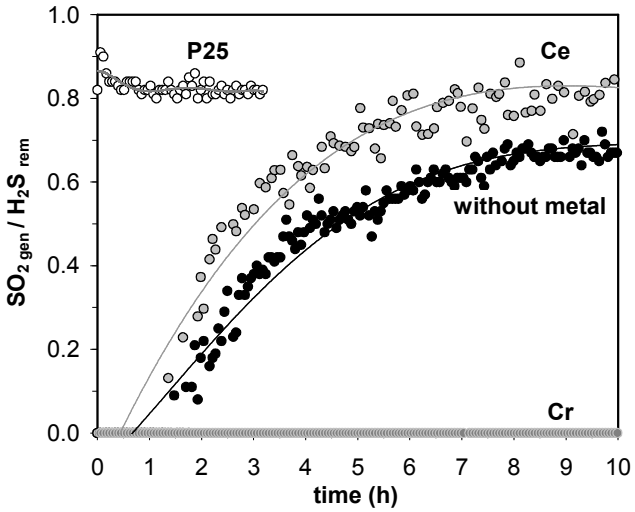
P25
Ce
without metal
Cr
$SO_{2\,gen}$ / H_2S_{rem}
time (h)
0.0
0.2
0.4
0.6
0.8
1.0
0
1
2
3
4
5
6
7
8
9
10

Figure 10

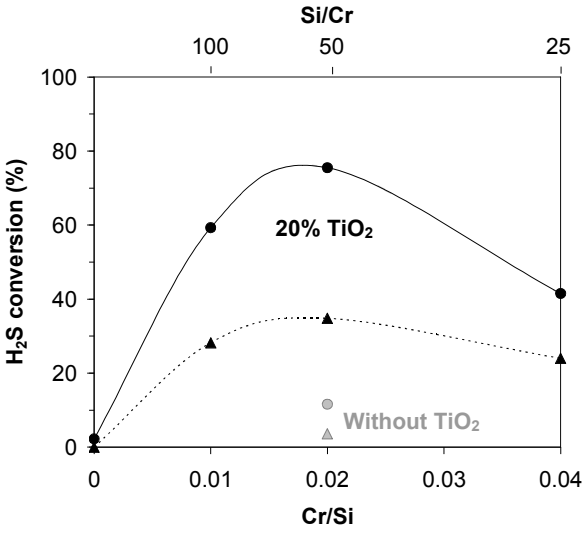
Si/Cr
100
50
25
100
80
60
40
20
0
H2S conversion (%)
20% TiO2
Without TiO2
0
0.01
0.02
0.03
0.04
Cr/Si